PAPER

Thickness dependence of the magnetic anisotropy and dynamic magnetic response of ferromagnetic NiFe films

To cite this article: E F Silva *et al* 2017 *J. Phys. D: Appl. Phys.* **50** 185001

IOP Publishing Journal of Physics D: Applied Physics

J. Phys. D: Appl. Phys. **50** (2017) 185001 (13pp) https://doi.org/10.1088/1361-6463/aa6665

Thickness dependence of the magnetic anisotropy and dynamic magnetic response of ferromagnetic NiFe films

E F Silva[1,2], M A Corrêa[1], R D Della Pace[3,4], C C Plá Cid[3], P R Kern[4], M Carara[4], C Chesman[1], O Alves Santos[2], R L Rodríguez-Suárez[2,5], A Azevedo[2], S M Rezende[2] and F Bohn[1]

[1] Departamento de Física, Universidade Federal do Rio Grande do Norte, 59078-900 Natal, RN, Brazil
[2] Departamento de Física, Universidade Federal de Pernambuco, 50670-901 Recife, PE, Brazil
[3] Departamento de Física, Universidade Federal de Santa Catarina, 88040-900 Florianópolis, SC, Brazil
[4] Departamento de Física, Universidade Federal de Santa Maria, 97105-900 Santa Maria, RS, Brazil
[5] Facultad de Física, Pontificia Universidad Católica de Chile, Casilla 306, Santiago, Chile

E-mail: felipebohn@fisica.ufrn.br

Received 21 November 2016, revised 8 March 2017
Accepted for publication 13 March 2017
Published 3 April 2017

Abstract

We investigate the thickness dependence of the magnetic anisotropy and dynamic magnetic response of ferromagnetic NiFe films. We go beyond quasi-static measurements and focus on the dynamic magnetic response by considering three complementary techniques: the ferromagnetic resonance, magnetoimpedance and magnetic permeability measurements. We verify remarkable modifications in the magnetic anisotropy, i.e. the well-known behavior of in-plane uniaxial magnetic anisotropy systems gives place to a complex magnetic behavior as the thickness increases, and splits the films in two groups according to the magnetic properties. We identify magnetoimpedance and magnetic permeability curves with multiple resonance peaks, as well as the evolution of the ferromagnetic resonance absorption spectra, as fingerprints of strong changes of the magnetic properties associated to the vanishing of the in-plane magnetic anisotropy and to the emergence of non-homogeneous magnetization configuration, local anisotropies and out-of-plane anisotropy contribution arisen as a consequence of the non-uniformities of the stress stored in the film as the thickness is increased and/or to the columnar growth of the film. We interpret the experimental results in terms of the structural and morphological properties, quasi-static magnetic behavior, magnetic domain structure and different mechanisms governing the magnetization dynamics at distinct frequency ranges.

Keywords: ferromagnetic films, magnetization dynamics, magnetic anisotropy

(Some figures may appear in colour only in the online journal)

1. Introduction

Investigation of the magnetization dynamics in systems with reduced dimensions is of fundamental importance to understand the basic physical properties of these systems as well as to provide new roads to applications. The discovery of novel materials and the exploration of the dynamic magnetic response in diverse systems has provided the development and optimization of a wide range of technological devices in recent decades [1–3]. This is especially true for ferromagnetic films, which are employed in a variety of magnetic sensors [4, 5].

Nowadays, the progress in this field is highly driven by the emergence of magnetic devices operating at high frequency. In particular, spintronics devices and data storage applications are increasingly being used at frequencies comparable to the

natural ferromagnetic resonance frequency. The response in these systems depends strongly on the experimental conditions used to excite the magnetization dynamics, as well as the intrinsic and extrinsic properties of the material. In particular, complex magnetization dynamics relies on the anisotropy and non-uniformity of the magnetization, which are governed by structural properties of the samples. Thus, magnetic noise and unpredictable magnetic responses, which prevent simple and straightforward functioning of magnetic sensors, must be well understood [6–8]. This justifies the large efforts devoted to the development of soft magnetic materials with high magnetic homogeneity for very fast magnetic switching and/or high-frequency applications [6]. Experimentally, many techniques are available and may provide information on the magnetic properties and high-frequency magnetic response of ferromagnetic films. For instance, the ferromagnetic resonance (FMR) has proven to be one of the most powerful techniques for investigating magnetic thin films. It has been largely used to investigate intrinsic and extrinsic magnetic properties of these systems, in particular giving information on anisotropies, magnetization relaxation mechanisms and microscopic interactions. All these properties are fundamental to determine the magnetization dynamics in the saturated regime [9–16]. However, the FMR effect in non-saturated samples are rarely investigated, mainly due to the relative complexity of the magnetic configuration.

Aiming to investigate the dynamic properties in the unsaturated magnetization regime, the *ac* magnetic permeability and magnetoimpedance (MI) techniques arise as very useful tools to help in the understanding of fundamental properties [3]. In this sense, these techniques provide complementary information to the FMR experiment. The magnetoimpedance effect corresponds to the change of the real and imaginary components of electrical impedance of a ferromagnetic conductor caused by the action of a quasi-static magnetic field. For a general review on the effect, we suggest [17]. The effect has been extensively studied in previous decades in a wide range of magnetic systems. In most cases, the key to understanding and controling the MI effect lies in the knowledge of the transverse magnetic permeability which, in turn, depends on several structural and magnetic parameters, such as effective anisotropy, magnetic damping, crystalline structure, and the geometry and thickness of the sample [18]. Therefore, the magnetoimpedance effect and magnetic permeability measurements appear as versatile tools to investigate ferromagnetic materials, revealing key information on the magnetization dynamics over a wide range of frequencies and fields. It also provides further insights on unsaturated and even saturated magnetization states, resonant and non-resonant regimes, as well as on the magnetic anisotropy, uniformity of the magnetization [19], nature of interactions governing the magnetization dynamics and energy terms affecting the transverse permeability [17]. All these issues are of utmost importance for the understanding of the high-frequency magnetization switching of magnetic devices.

Therefore, the comprehension of the relations among thickness, magnetic anisotropy and dynamic magnetic response of ferromagnetic films becomes crucial, being a technological key for magnetic storage devices, high-speed response sensors and miniaturized systems that use thin film technology.

In this work, we report an experimental investigation of the magnetic properties and magnetization dynamics in ferromagnetic NiFe films with thicknesses in the range between 50 and 1000 nm. We go beyond quasi-static measurements and characterize the films employing three complementary techniques: the ferromagnetic resonance, magnetoimpedance and magnetic permeability measurements. Thus, we address the thickness dependence of the magnetic anisotropy and dynamic magnetic response of the films. We verify remarkable modifications of the magnetic anisotropy with thickness and split the films into two groups according to the magnetic properties. Besides, we show that the dynamic magnetic response in saturated and unsaturated states is very rich and strongly dependent on the thickness. We interpret the experimental results in terms of the structural and morphologial properites, quasi-static magnetic behavior, magnetic domain structure and different mechanisms governing the magnetization dynamics at distinct frequency ranges.

2. Experiment

The NiFe alloys, as Ni_xFe_{100-x} with $78 \leqslant x \leqslant 82$, are viewed as a prototype of soft magnetic material and represent an ideal system for basic investigations. Usually, they present polycrystalline structures, low coercivity, vanishing magnetocrystalline anisotropy, near-zero magnetostriction (for $x \approx 81$) and a low damping parameter [20]. For these reasons, they are widely employed as magnetic material in thin film applications.

Here, we perform experiments in a set of ferromagnetic films with nominal composition $Ni_{81}Fe_{19}$ and thicknesses of 50, 100, 150, 200, 250, 300, 400, 500, 750 and 1000 nm. The NiFe films are deposited by magnetron sputtering onto glass substrates with dimensions of 10×4 mm^2. The deposition process is carried out with the following parameters: base vacuum of 10^{-7} Torr, deposition pressure of 2.0×10^{-3} Torr with a 99.99% pure Ar at 32 sccm constant flow, and using a 50 W DC power supply. Using these conditions, the deposition rate is 0.41 nm s^{-1}. During the film deposition, the substrate is submitted to a constant and homogeneous in-plane magnetic field with a magnitude of 1.5 kOe, applied perpendicularly to its main axis, in order to induce a magnetic anisotropy and define an easy magnetization axis. Figure 1 shows a schematic representation of a ferromagnetic NiFe film and the directions of the magnetic fields employed in the experiments. Additionally, to improve the film uniformity, the substrate moves at constant speed through the plasma. However, this procedure may induce additional effects due to the variation of the incidence angle [6, 21, 22], such as tilted columnar growth of the film.

The structural and morphological characterization is obtained by x-ray diffraction and transmission electron microscopy. X-ray diffraction experiments are performed using CuK_α radiation. While low-angle x-ray diffraction is employed to determine the deposition rate and calibrate the film thickness, high-angle x-ray diffraction measurements

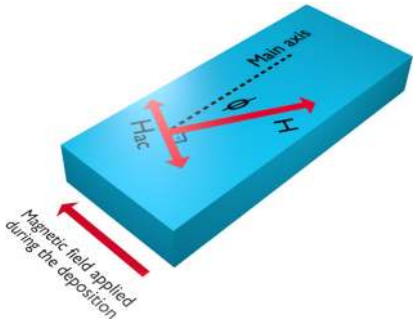

Figure 1. Schematic representation of a ferromagnetic NiFe film, where the in-plane magnetic field applied during the deposition is perpendicular to the main axis of the substrate, and the directions of the magnetic fields employed in the magnetization, FMR, MI and magnetic permeability experiments. All experiments are performed with the fields in the plane of the film. Notice that for the dynamic magnetic characterization, the respective alternating magnetic field H_{ac} is always transverse to the orientation of the quasi-static magnetic field H. Here, we define ϕ as the angle between H and the main axis of the film.

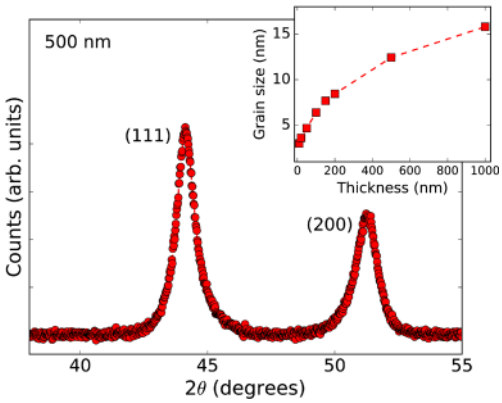

Figure 2. High angle x-ray diffraction pattern for the NiFe film with thickness of 500 nm. The (1 1 1) and (2 0 0) NiFe peaks are identified at $2\theta \approx 44.2°$ and $2\theta \approx 51.5°$, respectively, indicating the polycrystalline state of the film. The films with distinct thicknesses present similar behavior. The inset shows the evolution of the grain size as a function of the film thickness.

are used to verify the structural character of the samples. Moreover, further structural information is provided by cross-section transmission electron microscopy, in the bright and dark field imaging modes, as well as with selected electron area diffraction technique, obtained with a JEOL-2100 transmission electron microscope.

All the experiments in this study are performed at room temperature. The in-plane magnetic properties are obtained through magnetization curves, measured with a vibrating sample magnetometer, with the magnetic field H applied both along ($\phi = 0°$) and perpendicular ($\phi = 90°$) to the main axis of the films. To obtain further information on the magnetic behavior and magnetic domain morphology, images of the domain structure of the films are acquired using high-resolution longitudinal Kerr effect experiments and magnetic force microscopy. In particular, all images are taken at the remanence, after in-plane magnetic saturation.

The dynamic magnetic response of the films is investigated through three techniques: FMR, MI, and magnetic permeability measurements. The techniques use the same magnetic fields configuration, in which the sample is simultaneously submitted to a magnetic field H and a transverse alternating magnetic field with amplitude H_{ac} and frequency f. Here, following the quasi-static magnetic characterization, we define ϕ as the angle between H and the main axis of the film, as shown in figure 1.

The FMR experiment is performed using a homemade X-band spectrometer operating at 9.5 GHz. The sample is mounted on the tip of an external goniometer and inserted in the center of a TE_{102} rectangular microwave cavity, with Q factor of 2500 and an oscillator-cavity frequency stabilization circuit. The quasi-static magnetic field H, applied in the plane of the film, varies from 0.6 up to 1.6 kOe. Helmholtz coils on the cavity walls modulate the field at 99 kHz, allowing the lock-in detection of the derivative of the absorption spectra. The set up allows the rotation of the sample. Thus, the resonance field H_R as a function of the angle ϕ is determined by fitting the derivative of the absorption spectra. For further details on the experiment and analysis, we recommend [13, 23, 24].

The MI effect is measured using a *rf*-impedance analyser Agilent model *E*4991, with *E*4991*A* test head connected to a microstrip in which the sample is the central conductor, separated from the ground plane by the substrate. The electric contacts are made with low resistance silver paint. To avoid propagation effects and acquire just the sample's contribution to MI, the analyser is calibrated at the end of the connection cable by performing open, short and load (50 Ω) measurements using standard references. The alternating electric current i_{ac} and quasi-static magnetic field H are both along the main axis of the film, $\phi = 0°$. MI measurement is taken over a frequency range between 0.5 and 3.0 GHz, with a maximum field of ±350 Oe. While the magnetic field is varied, a 0 dBm (1 mW) constant power is applied to the sample, characterizing a linear regime of driving signal. Thus, at a given field value, the frequency sweep is made and the real R and imaginary X components of the impedance Z are simultaneously acquired. The dispersion relation curve, i.e. the resonance frequency for each magnetic field value, is obtained from the usual procedure of plotting the position in frequency of the peaks of the R component, located at the same frequency of the zero crossing of the X one, for each magnetic field value. For further information on the whole experimental procedure, we suggest [18].

The magnetic permeability results are obtained using an experimental setup based on the transmission line perturbation method, in which the sample is inserted in a segment of a transmission line, leading to changes of characteristic parameters of the whole system, such as impedance, permittivity and effective magnetic permeability. Measurements of the reflection coefficient S11 are performed using a vector network analyser Rohde & Schwarz model ZVB14. The microstrip is constructed directly on the SMA *rf* connector [25] with a characteristic impedance of ≈50 Ω. The line length is 6.5 mm and the upper line and ground plate separation is 0.5 mm, twice the substrate thickness. Similarly to the MI measurement, the microstrip line and quasi-static

magnetic field H are along the main axis of the film, $\phi = 0°$. The permeability measurements are taken over a wide frequency range, from 0.05 up to 7.0 GHz, with a maximum field of ± 220 Oe. Initially, the analyser is also calibrated at the end of the connection cable by performing the open, short and load (50 Ω) measurement procedures. To the measurements, the calibration plane is dislocated to the beginning of the microstrip line. The real μ' and imaginary μ'' components of the magnetic permeability μ are determined through an analytical approach from the measurements of the reflection coefficient S11 of the microstrip line when empty, loaded with a substrate with the same dimensions of the sample, and with the own sample, following the procedure discussed in detail in [25, 26]. The dispersion relation curve is obtained by considering a procedure very similar to that performed for the MI results. However, here, the typical behavior for ferromagnetic resonance is found by plotting the position in frequency of the μ'' component of the magnetic permeability, which occurs simultaneously to the zero crossing of the μ'' one, for each magnetic field value [6].

3. Results and discussion

We first characterize the films from the structural and morphological point of views. Following, we investigate the quasi-static magnetic behavior. This shows remarkable modifications in the magnetic anisotropy and magnetic properties (hysteresis loops, coercive fields, etc) with the thickness. In a third moment, we investigate the dynamic magnetic response through three distinct and complementary techniques. The dynamic magnetic characterization reveals the increase of the complexity of the whole sample as the film thickness is raised.

3.1. Structural and morphological characterization

Structural and morphological characterization is obtained by x-ray diffraction and transmission electron microscopy. Figure 2 shows the high-angle x-ray diffraction pattern for the film with a thickness of 500 nm. Similar behavior is verified for the films with different thicknesses. In this case, the pattern indicates the polycrystalline state of all films, assigned by the well-defined and high-intensity (1 1 1) and (2 0 0) NiFe peaks, identified at $2\theta \approx 44.2°$ and $2\theta \approx -51.5°$, respectively. No evidence of evolution of the texture is verified with thickness, i.e. although the peaks have an increase of intensity as the films become thicker as expected, the relative intensity between them keeps invariant. However, the width of the peaks decreases as the thickness increases, revealing the raise of the grain size. In particular, the grain size calculated from the width at the half height of the (1 1 1) peak using the Scherrer method [27] remains between 3 and 16 nm, as shown in the inset of figure 2.

Figure 3 presents the results of transmission electron microscopy for the film with thickness of 50 nm, as a representative example of the general features verified for this set.

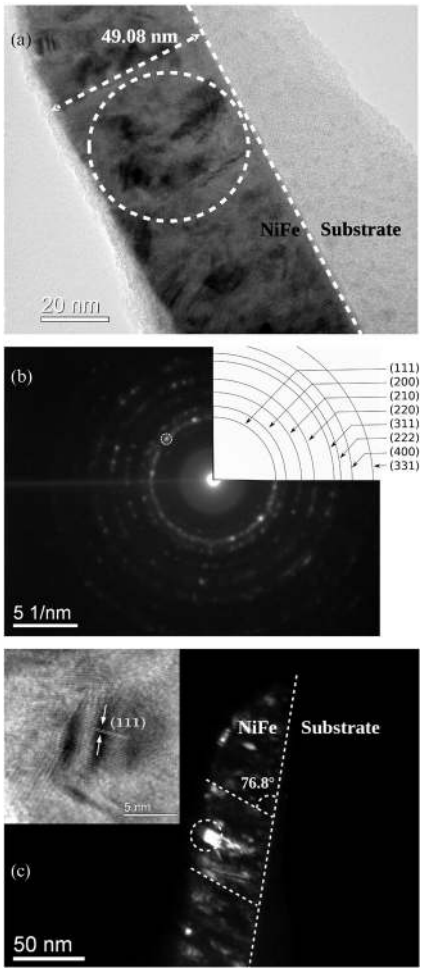

Figure 3. Results of transmission electron microscopy for the film with thickness of 50 nm. (a) Bright field cross-section transmission electron microscopy image. The white circle shows the limits of the area investigated through the diffraction technique. (b) Selected electron area diffraction pattern, where the diffraction rings with interplanar spacings d_{hkl} matching to the (1 1 1), (2 0 0), (2 1 0), (2 2 0), (3 1 1), (2 2 2), (4 0 0) and (3 3 1) planes of NiFe are observed. The standard pattern and d_{hkl}-spacings for the NiFe alloy are obtained from the CIF 01-071-8324. The acquired pattern confirms the polycrystalline state of the film previously verified through the high-angle x-ray diffraction results. The white circle in (b) indicates the diffraction spot considered to the obtainment of the dark field image presented in the following. (c) Dark field image obtained from the spot of the (1 1 1) NiFe plane. The white circle delimits the part of the sample in which the high-resolution images are taken. In the inset, the high-resolution transmission electron microscopy image reveals the tilted columnar growth of the film, in which the $\langle 1\,1\,1 \rangle$ direction has an inclination angle of about 13.2° with respect to the normal of the substrate. The films with distinct thicknesses present similar features as well.

Figure 3(a) shows the bright field cross-section transmission electron microscopy image. Besides probing the morphology and structural character of the material, the transmission electron microscopy images confirm the thickness of the films. In particular, differences smaller than 2% with respect to the nominal thickness are found, placing the sputtering as a reliable technique to produce reproducible samples. Selected electron area diffraction analysis, shown in figure 3(b), discloses

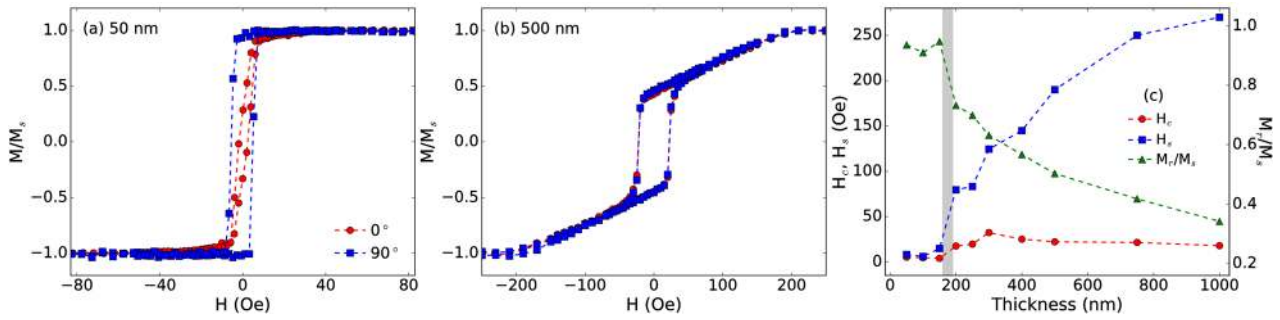

Figure 4. ((a) and (b)) Normalized magnetization curves for the NiFe films with thicknesses of 50 and 500 nm, measured with the magnetic field H applied along ($\phi = 0°$) and perpendicular ($\phi = 90°$) to the main axis of the films. For this set of films, a change of magnetic behavior is verified in the thickness range between 150 and 200 nm. Films with thicknesses below 150 nm present behavior similar to that of the 50 nm-thick film, typical of an in-plane uniaxial magnetic anisotropy system, while the films above 200 nm have the same features observed for the film with thickness of 500 nm, i.e. isotropic in-plane magnetic properties, with an out-of-plane anisotropy contribution. (c) Coercive field H_c, saturation field H_s and normalized remanent magnetization M_r/M_s, obtained from the magnetization curves measured for $\phi = 90°$, as a function of the film thickness. The gray zone represents the critical thickness range, which splits the films into two groups according to the magnetic behavior.

a typical pattern of a polycrystalline material, assigned by the presence of diffraction rings with interplanar spacings d_{hkl} matching to the (1 1 1), (2 0 0), (2 1 0), (2 2 0), (3 1 1), (2 2 2), (4 0 0) and (3 3 1) planes of NiFe, in agreement with d_{hkl}-spacing for a face-centered cubic fm-3m space group. Moreover, it is possible to note the presence of spots indicating some degree of preferential growth direction, being the most intense spots associated with the (1 1 1) NiFe plane, corroborating the high-angle x-ray diffraction results. Figure 3(c) presents a dark field image obtained from the spot of the (1 1 1) NiFe plane shown in figure 3(b). The bright regions uncover that the film is formed by columns with different growth directions. In the inset, the high resolution transmission electron microscopy image from the diffracted region reveals the tilted columnar growth, in which the ⟨1 1 1⟩ direction has an inclination angle of about 13.2° with respect to the normal of the substrate.

3.2. Quasi-static magnetic characterization

Quasi-static magnetic characterization is obtained through magnetization curves. Figures 4(a) and (b) show the magnetization curves, measured with the magnetic field, both applied along and perpendicular to the main axis, obtained for NiFe films with selected thicknesses. And figure 4(c) presents the thickness dependence of the coercive field H_c, saturation field H_s and normalized remanent magnetization M_r/M_s, obtained from the magnetization curves measured for $\phi = 90°$.

When analysed as a function of the thickness, an evolution in the shape of the magnetization curves is noticed, indicating the existence of a critical thickness range, which splits the films into two groups according to the magnetic properties. Here, the change of magnetic behavior is verified in the range between 150 and 200 nm.

Films below 150 nm exhibit behavior of a classical in-plane uniaxial magnetic anisotropy system [28]. The angular dependence of the curves indicates a well-defined in-plane uniaxial magnetic anisotropy, without any out-of-plane component, induced by the magnetic field applied during the deposition. For $\phi = 90°$, a square loop is acquired, since the magnetic field is along the induced easy magnetization axis. The films have low H_c values, and this coercivity is primarily related to the uniaxial anisotropy and to the existence of pinning centers for the domain walls due to the surface irregularities [29]. The domain wall motion is the main mechanism acting during the magnetization reversal, a fact revealed by the own shape of the curve and by the almost constant values of $H_s \approx H_c$ and $M_r/M_s \approx 0.97$. On the other hand, for $\phi = 0°$, a slightly tilted loop with low remanence appears once the magnetic field is perpendicular to the easy axis. The non-zero coercive field and area of the magnetization curve are evidences of the existence of some dispersion of the magnetic anisotropy [30]. Reversible and irreversible rotations of the magnetization are the main responsibles by the magnetization reversal process.

The magnetic properties of these films and the main features of the magnetization curves are well described by a modified Stoner–Wohlfarth model [30–33], previously studied by our group, which mimics anisotropic systems with magnetic anisotropy dispersion. In particular, based on numerical calculations performed with the theoretical approach for a system with effective uniaxial magnetic anisotropy, the films below 150 nm can be characterized by the saturation magnetization of $M_s \approx 780$ emu cm^{-3} and anisotropy field H_k values in the range between 5 and 10 Oe, corresponding to values of effective anisotropy constant $K_{eff} = \frac{1}{2}M_s H_k$ from ≈1.9 up to ≈3.9 kerg cm^{-3}, values compatible with those found in literature for Permalloy films [34–36].

Regarding the magnetic domain structure, figure 5(a) depicts the domain pattern verified for the films thinner than 150 nm. In particular, it is well-known that the magnetic structure for films, within this thickness range and with in-plane uniaxial magnetic anisotropy, is characterized by large in-plane domains with antiparallel magnetization oriented along the easy axis, separated by various types of domain walls (Néel, cross-tie, asymmetric Néel, and Bloch walls) strongly dependent on the film thickness [6, 36–39].

On the other hand, films above 200 nm have isotropic in-plane magnetic properties, with an out-of-plane anisotropy

contribution [26, 36–40]. The remarkable change in the shape of the magnetization curves reveals the deterioration of the soft magnetic properties observed for the thinner films. The curves are unchanged whatever the orientation of the applied in-plane magnetic field, a fingerprint of the so-called rotatable anisotropy effect [36, 37, 40]. Moreover, they are characterized by an abrupt magnetization reversal at fields close to the coercive field, occurring mainly through domain wall motion, followed by a linear approach to the magnetic saturation, in which the main magnetization reversal mechanism becomes the magnetization rotation.

The observed behavior is essentially related to the stress stored in the film as the thickness is increased and/or to the tilted columnar growth arisen due to the oblique incidence of the sputtered particles during the deposition [6, 21, 22, 34, 41], the latter clearly evidenced in figure 3(c). The characteristic shape of the magnetization curve appears to result from the juxtaposition of both hard and soft magnetic regions of a non-homogeneous magnetic system [6]. The initial increase of H_c with thickness is attributed to the formation of stress centers in the bulk of the samples during the growth process [29]. The further decrease is related to the higher contribution of the magnetization rotation to the magnetization reversal process, due to local anisotropies and perpendicular anisotropy. This contribution is also responsible for the loss of the square shape of the magnetization curves, resulting in a noticeable decrease of M_r/M_s and considerable increase of H_s. In particular, the latter is directly connected to the value of the perpendicular anisotropy $K_\perp = \frac{1}{2}M_sH_s$ [39], since the anisotropy field H_k can be estimated at the field at which rotations start appearing, considering the curve coming from saturation [42]. Thus, by assuming $M_s = 780$ emu/cm^3, the out-of-plane anisotropy constant presents values in the range between ≈29 and ≈102 kerg cm^{-3}.

Concerning the magnetic domain structure in the films thicker than 200 nm, the emergence of rotatable magnetic anisotropy and out-of-plane anisotropy contribution, as well as the general magnetic behavior and characteristic shape of the magnetization curve, uniquely indicates the presence of a stripe magnetic domains pattern [6, 36, 37, 39, 40, 43–45]. They are clearly evidenced in figure 5(b). The period of the stripes is comparable to the film thickness [37, 39]. It is known that the stripe domain structure is established by applying a magnetic field high enough to magnetically saturate the film along an in-plane direction, and then reducing the field to zero [37]. As a consequence of the stripe domains, an induced rotatable anisotropy appears as a pseudo-uniaxial anisotropy aligned along the direction of the stripes [36, 46]. Its magnitude is comparable or even much higher than the one of the uniaxial anisotropy induced by the magnetic field applied during the deposition, as previously shown.

Similar dependence of the magnetic behavior with thickness has been already verified by several groups, considering samples with different compositions and using distinct experimental techniques [6, 26, 36–40, 46–52]. For our set of NiFe films, as aforementioned, the change of magnetic behavior is found to occur between 150 and 200 nm. However, we point out that this critical thickness range is strongly dependent on the preparation conditions of the films, such as substrate, pressure and power deposition, as well as on the own composition of the alloy, since this latter affects magnetic parameters as the magnetostriction constant and magnetocrystalline anisotropy [46, 52]. For these reasons, reports indicating distinct critical thickness ranges may be found in literature [26, 36, 40, 46, 47]. Anyway, the interpretation for the dependence of the magnetic behavior with the film thickness is common for all studies. The change of the magnetic behavior with thickness is usually associated to a competition between the planar demagnetization energy, the shape anisotropy energy, magnetoelastic energy and the domain wall energy [53]. Thus, for the films with thicknesses below the critical thickness range, the magnetic field applied during the deposition and the planar demagnetization energy term are mainly responsible for the in-plane and uniaxial magnetic anisotropies [53]. In the case of the films with thicknesses above this range, the in-plane magnetic anisotropy is obscured by the local stress stored in the film during deposition, as well as by the emergence of local anisotropies and non-homogeneous magnetization configuration as the thickness increases. Besides, it is verified that the tilted columnar growth, due to oblique incidence of the sputtered particles, can also be responsible for creating an effective out-of-plane perpendicular magnetic anisotropy contribution [6, 21, 22, 34, 40, 41].

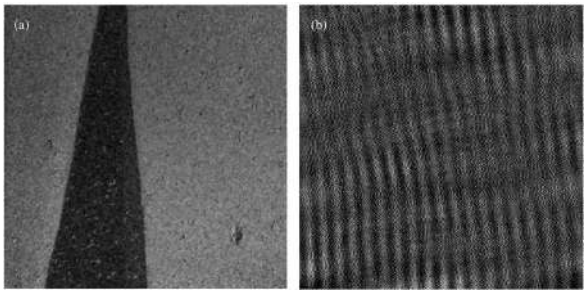

Figure 5. Magnetic domain structure for the NiFe films with thicknesses of (a) 100 and (b) 200 nm. Films with thicknesses below 150 nm present a domain structure similar to that of the 100 nm-thick film, characterized by large in-plane domains with antiparallel magnetization oriented along the easy axis. Within this thickness range, the images are acquired by high-resolution longitudinal Kerr effect experiments and the image size is 400×400 μm^2. The films above the critical thickness range have the same features observed for the 200 nm-thick film, which presents stripe domain structure. For this thickness range, the images are acquired by magnetic force microscopy and the image size is 30×30 μm^2. All images are taken at the remanence, after in-plane magnetic saturation. Specifically considering these images, the field is applied along the vertical direction.

3.3. Dynamic magnetic response

The quasi-static magnetic properties play a fundamental role on the magnetization dynamics. Thus, strong modifications in dynamic magnetic response are expected as the film thickness is varied. Here, the dynamic measurements are carried out by the FMR, MI and magnetic permeability experiments.

Figure 6 shows the derivative of the FMR absorption spectra, measured with the in-plane magnetic field H, both

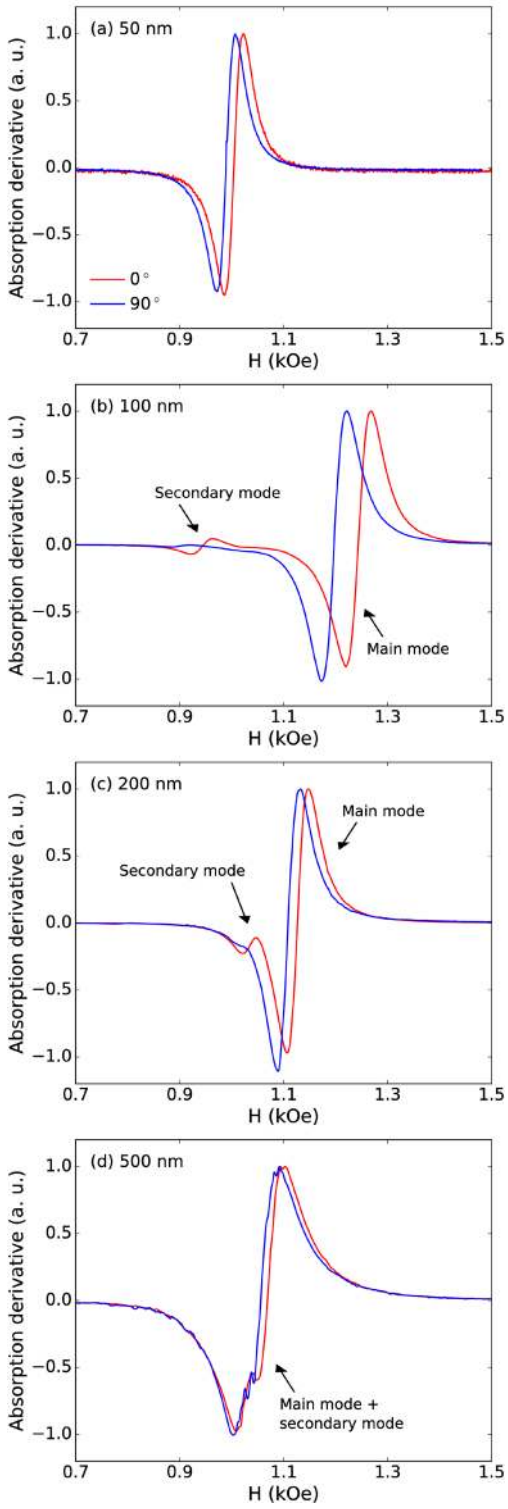

Figure 6. Derivative of the FMR absorption spectra for NiFe films with selected thicknesses at resonance frequency $f_r = 9.5$ GHz. Although the curves are acquired for several ϕ values, just the results for $\phi = 0°$ and 90° are shown here in order to make the visualization clearer.

applied along and perpendicular to the main axis of the samples, for NiFe films with selected thicknesses. Interesting features related to the shape of the resonance spectra reside in the dependence on the number of resonance modes, as well as on the amplitude and position of the modes, with the film thickness.

With respect to the number of modes, the 50 nm-thick film presents spectra with a single FMR mode. Although measurements were performed considering wider magnetic field ranges, no evidence of further resonance modes is observed. In particular, this behavior with a single FMR mode is expected for single systems with homogeneous in-plane magnetization configuration, as observed in most films with in-plane uniaxial anisotropy and polycrystalline structure [13, 36, 46, 54, 55].

Thicker films have spectra with two resonance modes, with distinct amplitudes and variable separation. The resonance mode with higher amplitude corresponds to the well-known main precession mode, while the smaller one is attributed to a secondary resonance mode [54].

The secondary mode has fingerprints of a perpendicular standing spin wave (PSSW) mode [56, 57]. For the films with thicknesses of 100 and 150 nm (the latter not shown here), which still present in-plane uniaxial magnetic anisotropy, the secondary resonance mode may be associated to non-homogeneous magnetization configuration and some dispersion of the magnetic anisotropy. Despite the similar magnetic behavior, these films have slightly higher anisotropy dispersion if compared with the 50 nm-thick film, a fact related to the local stress stored in the film as the thickness increases. For the films with thicknesses above 200 nm, presenting isotropic in-plane magnetic properties and out-of-plane magnetic anisotropy contribution, the secondary resonance mode in turn is a response of regions with local anisotropies originated from the non-uniformity of the stress [6]. In particular, similar FMR spectra are characteristic of systems with non-homogeneous magnetization configuration [15, 54, 56, 57].

Regarding the amplitude and position of the resonance modes, both are strongly dependent on the magnetic behavior and on the film thickness. The main resonance mode has much higher amplitude than the secondary resonance one, as expected [58]. Moreover, an evolution in the position of the resonance modes as the thickness increases can be noticed. Considering $\phi = 0°$, the spectrum with the single resonance mode, located at ≈ 1.0 kOe, observed for the 50 nm-thick film initially evolves to a pattern with two well-defined and separated resonance modes, located at $\approx$0.95 and $\approx$1.20 kOe, verified for the film with thickness of 100 nm. A continuous displacement of both resonance modes toward $\approx$1.07 kOe is verified as the films become thicker, following the modifications of the quasi-static magnetic properties. The films with 100 and 150 nm (the latter not shown), with in-plane magnetic anisotropy, still present separated resonance modes. However, as a signature of the change of magnetic anisotropy and the emergence of isotropic in-plane magnetic properties, the resonance modes start overlapping, evidenced in the curve for the 200 nm-thick film, and merge, as identified for the film with 500 nm, as the thickness increases.

From the derivative of the FMR absorption spectra, figure 7 shows the in-plane angular dependence of the resonance field H_R and the FMR linewidth ΔH of the main precession

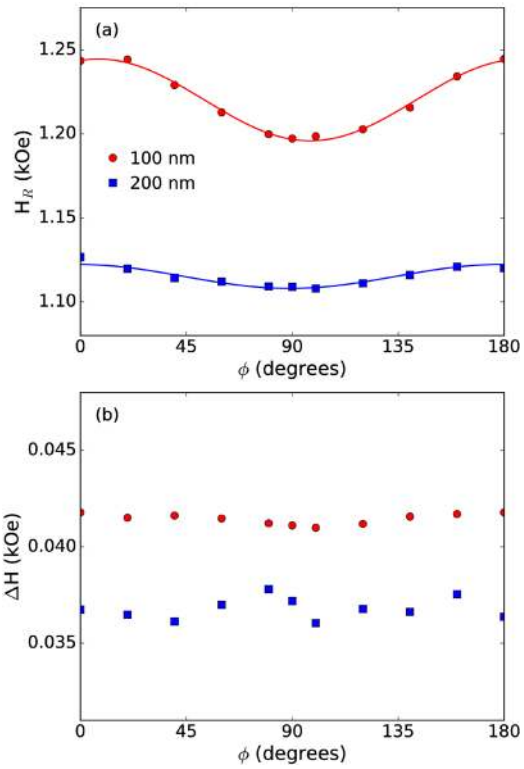

Figure 7. In-plane angular dependence of (a) the resonance field H_R and (b) the FMR linewidth ΔH of the main precession mode, with $f_r = 9.5$ GHz, for the NiFe films with thicknesses of 100 and 200 nm, as representative examples of the films with distinct quasi-static magnetic behaviors. In (a), the solid lines, red and blue, are the theoretical fits obtained from relation (2) and by using the appropriate magnetic free energy term for an uniaxial anisotropy system, following the procedure described in [13].

mode for NiFe films with selected thicknesses, as representative examples of the films with distinct quasi-static magnetic behaviors.

The in-plane angular dependence of the FMR linewidth ΔH for both 100 and 200 nm-thick films is roughly constant, despite some fluctuations. Similar behavior is verified for all samples.

Regarding the resonance field, the in-plane angular dependence of H_R confirms that the 100 nm-thick film has a clear in-plane uniaxial magnetic anisotropy, with the easy magnetization axis oriented perpendicularly to the main axis (See figure 1). This feature is ascribed to the fact that the H_R reaches the maximum (minimum) value when H is perpendicular (parallel) to the easy magnetization axis. These cases are respectively identified for $\phi = 0°$ and 90°. Similar general behavior is verified for the all films with thicknesses below 150 nm, as expected.

Further, thicker films share curves of H_R as a function of the angle ϕ that are similar to that measured for the 200 nm-thick film. They are characterized by roughly constant H_R values, evidencing the in-plane magnetic isotropic behavior previously verified through the magnetization curves. The slight variation of the H_R values is a fingerprint of a residual uniaxial anisotropy induced by the magnetic field applied during the deposition, which is not completely obscured by the local stress stored in the film.

Table 1. Parameters obtained from the best fits to the experimental FMR data, at $f_r = 9.5$ GHz, for the NiFe films at selected thicknesses.

Thickness (nm)	$\langle \Delta H \rangle$ (Oe)	$4\pi M_{eff}$ (kG)
50	32	10.55
100	41	8.73
200	37	9.42
500	38	9.87

The equation for the resonance frequency can be expressed as a function of the second derivatives of the magnetic free energy, from the well-known Smith-Beljers relation [59, 60], and it is

$$f_r^2 = \left(\frac{\gamma}{2\pi}\right)^2 \frac{1}{M_s^2 \sin^2\theta_M}\left[\frac{\partial^2 E}{\partial\theta_M^2}\frac{\partial^2 E}{\partial\varphi_M^2} - \left(\frac{\partial^2 E}{\partial\theta_M \partial\varphi_M}\right)^2\right], \quad (1)$$

where f_r is the resonance frequency of the main precession mode, $\gamma = g\mu_B/\hbar$ is the gyromagnetic ratio associated to the effective g-Landé coefficient, θ_M and φ_M are the polar and azimuthal angles of the magnetization, respectively, at equilibrium magnetization configuration for a given value of the applied field, and E is the magnetic free energy density of the system.

Here, from equation (1), following the procedure described in [13] and considering the magnetic free energy for an uniaxial anisotropy system, the angular dependence of the resonance field H_R as a function of the anisotropy field H_k and effective magnetization $4\pi M_{eff}$ can be written as

$$H_R = (2\pi f_r/\gamma)^2/4\pi M_{eff} - 2H_k \sin^2\phi. \quad (2)$$

In particular, considering $f_r = 9.5$ GHz and $\gamma/2\pi = 2.94$ GHz kOe^{-1} [13, 61], for films with thickness below 150 nm, H_k values are found in the range between 7 and 24 Oe, in good agreement with the values previously verified from the quasi-static magnetic characterization.

The value of $4\pi M_{eff}$ varies significantly with the film thickness. A decrease from $4\pi M_{eff} = 10.55$ kG to 8.73 kG is verified as the thickness varies from 50 to 100 nm. Above 100 nm, the effective magnetization continuously increases with the thickness, reaching up to ≈9.9 kG for the thicker films. This latter variation of $4\pi M_{eff}$ is devoted to the reduction of the surface anisotropy, given that they are related through $4\pi M_{eff} = 4\pi M_s - 2K_s/M_s t$, where $2K_s/M_s t$ is the surface anisotropy field, K_s is the surface anisotropy constant, and t is the film thickness [62]. Similar behavior of $4\pi M_{eff}$ with thickness has been previously reported for Permalloy films and the values obtained here are consistent with those found in literature [35, 62–64].

Table 1 summarizes the mean values of FMR linewidth and effective magnetization for the NiFe films at selected thicknesses. The features evidenced by the FMR experiments are in agreement with the ones verified through the quasi-static magnetic characterization and are corroborated by the magnetoimpedance and magnetic permeability results.

Figures 8 and 9 show the general view of the impedance Z and relative magnetic permeability μ/μ_o for NiFe films

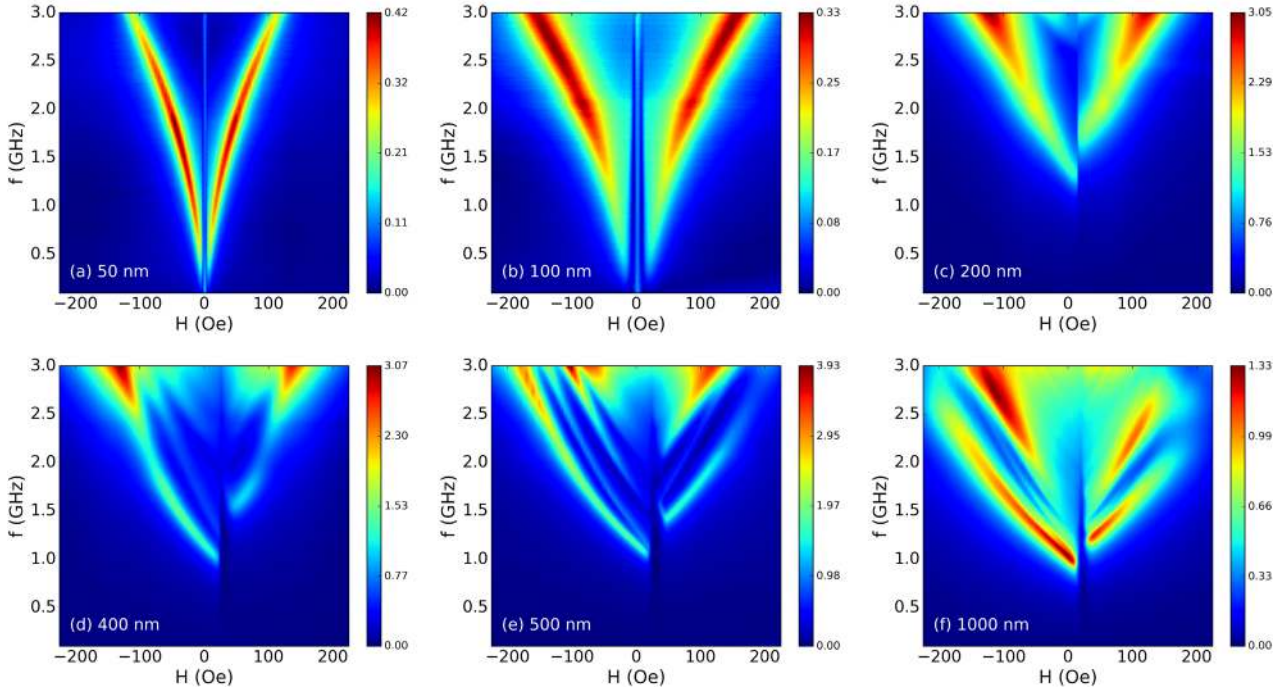

Figure 8. Two-dimensional plot of the impedance Z as a function of both quasi-static in-plane magnetic field H and frequency f for NiFe films with selected thicknesses. The curves are obtained for $\phi = 0°$. Although the curves are acquired over a complete magnetization loop and present hysteretic behavior, here we show just part of the curve, when the field goes from negative to positive values. Films with thicknesses below 150 nm present similar behavior, characteristic of typical uniaxial systems, while films above 200 nm present a complex magnetic behavior, depicted by several ferromagnetic resonance peaks detected at relatively low fields.

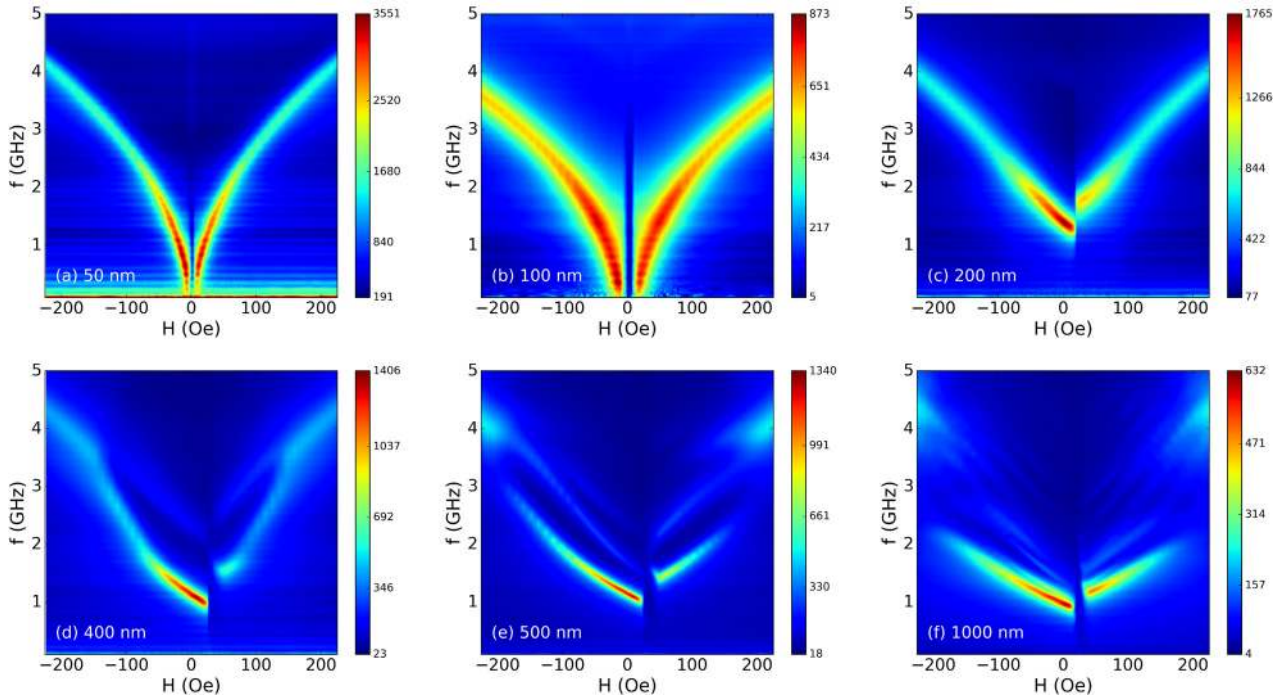

Figure 9. Two-dimensional plot of the relative magnetic permeability μ/μ_o as a function of both quasi-static in-plane magnetic field H and frequency f for NiFe films with selected thicknesses. The curves are obtained for $\phi = 0°$. The curves are acquired over a complete magnetization loop and present hysteretic behavior. Here we show just part of the curve, when the field goes from negative to positive values. Notice the remarkable similarities among the impedance Z and relative magnetic permeability μ/μ_o for each film thickness.

with selected thicknesses, obtained for $\phi = 0°$. By considering the two-dimensional plot, it is possible to observe the behavior of Z and μ/μ_o as a function of both quasi-static magnetic field H and frequency f. In particular, the magnetoimpedance and magnetic permeability curves are acquired over a complete magnetization loop and present hysteretic behavior. However, here we show just part of the curves, in which the measurements start from the negative field, with amplitude high enough to magnetically saturate the films, followed by the quasi-static sweep of the field up to the maximum positive value. When the field goes from positive to negative values, the behavior of both curves is reversed, a feature associated to the magnetization reversal process in the descending branch of the magnetization loop. From the figures, notice the striking similarity among the results provided by these techniques, a fact that is not a surprise since electrical impedance and magnetic permeability are closely related [31, 33].

Films below 150 nm present the well-known symmetric behavior around $H = 0$ of anisotropic systems, including the dependence with the magnetic field amplitude, frequency and the orientation of the quasi-static magnetic field H and alternating magnetic field H_{ac} with respect to the magnetic anisotropies [33]. The curves have a double peak structure[6] for the whole frequency range, a feature of the FMR relation dispersion for an uniaxial magnetic anisotropy system [32, 65, 66], in a signature of the simultaneous alignment the alternating magnetic field with the easy magnetization axis, and perpendicular alignment of the quasi-static magnetic field H with the same easy axis [67].

For frequencies below 0.15 GHz, the double peak behavior is not clearly observed, due to the reduced thickness of the films and to the very low Z and μ/μ_o variations. For frequencies of ≈0.5 GHz, the peaks appear and are located close to the anisotropy field H_k. This feature relates, in the first moment, the quasi-static and dynamical magnetic properties. For frequencies beyond this value, the FMR effect becomes an important mechanism responsible by the Z and μ/μ_o variations, a fact evidenced by the displacement of the position of the peaks in the double peak structure toward higher fields as the frequency is increased, following the behavior predicted by the FMR dispersion relation [65, 66]. This contribution of the FMR effect is also confirmed using the method described by Barandiarán *et al* [68] and previously employed by our group [48].

The resonance peaks in the double peak structure, for a given frequency, can be associated to the main resonance mode [36] previously observed in the FMR experiment. The emergence and raise of some dispersion of the magnetic anisotropy are evidenced here by the width of the peaks, which are verified wider for the film with thicknesses of 100 and 150 nm (the latter not shown here) when compared to the results for the 50 nm-thick film.

[6] Notice that, in the context of magnetoimpedance and magnetic permeability experiments, the terminology 'double peak structure' refers to curves that present two resonance peaks, i.e. one peak located at negative field values and another at positive field ones.

In contrast to the spectra of the films below 150 nm, the films with thicknesses above 200 nm present complex magnetic behavior, depicted by several resonance peaks detected at relatively low fields. The displacement of the position of each peak in the multiple peaks structure toward higher fields as the frequency is increased confirms the ferromagnetic resonance effect as the main mechanism responsible for the Z and μ/μ_o variations.

In particular, even the films thicker than 200 nm present an out-of-plane anisotropy contribution, the several resonance peaks are not interpreted in terms of perpendicular standing spin waves. This is justified since the frequency range employed in these experiments is much smaller than that in which these waves are usually observed [69]. Also, the resonance peaks seem not to be quantized, a required condition for the appearance of standing spin waves [70].

In this sense, the multiple resonance peaks are associated to regions with local anisotropies originated from the non-uniformity of the stress [6], as well as to different spin regions (part of domains, closure domains and domain walls) of the stripe domains [36, 46, 52]. This fact becomes plausible since the films are in an unsaturated state. Moreover, given that each region responds independently to the alternating magnetic field, the raise of the number of resonance peaks is consistent to the expected increase of the whole system complexity with thickness.

The ferromagnetic resonance peaks can also be analyzed through the field dependence of the resonance frequency, i.e. considering the dispersion relations determined from equation (1). Since the techniques employed here share the same field configuration, it is expected that equation (2) can also be employed to describe the relation between resonance frequency f_r and quasi-static magnetic field H. Considering only high-field data, where the contribution of the anisotropy field can be neglected, i.e. $4\pi M_{eff} \gg H$, it predicts a straight line with zero intercept for the plot of f_r^2 versus H which can be expressed by

$$f_r^2 \approx (\gamma/2\pi)^2 H 4\pi M_{eff}, \tag{3}$$

whose slope is determined by the effective magnetization of the material [18].

Figure 10 shows the dispersion relations obtained from the results of the impedance Z and relative magnetic permeability μ/μ_o, $\phi = 0°$, for NiFe films with selected thicknesses.

Films below 150 nm present a typical behavior of ferromagnetic resonance, which obeys a linear relation with the straight line fit passing through the origin. Thus, in this case, the fits corroborate the decrease of the effective magnetization previously verified through the FMR experiment. A change from $4\pi M_{eff} \approx 9$ to 7 kG is obtained as the thickness varies from 50 to 100 nm, such that a good agreement of the $4\pi M_{eff}$ values determined through the three techniques can be found.

For films with thicknesses above 200 nm, the dispersion relations deviate from the single linear behavior. A non-linear relationship between f_r^2 and H occurs at fields below H_s, since the magnetization is not a constant value and is strongly

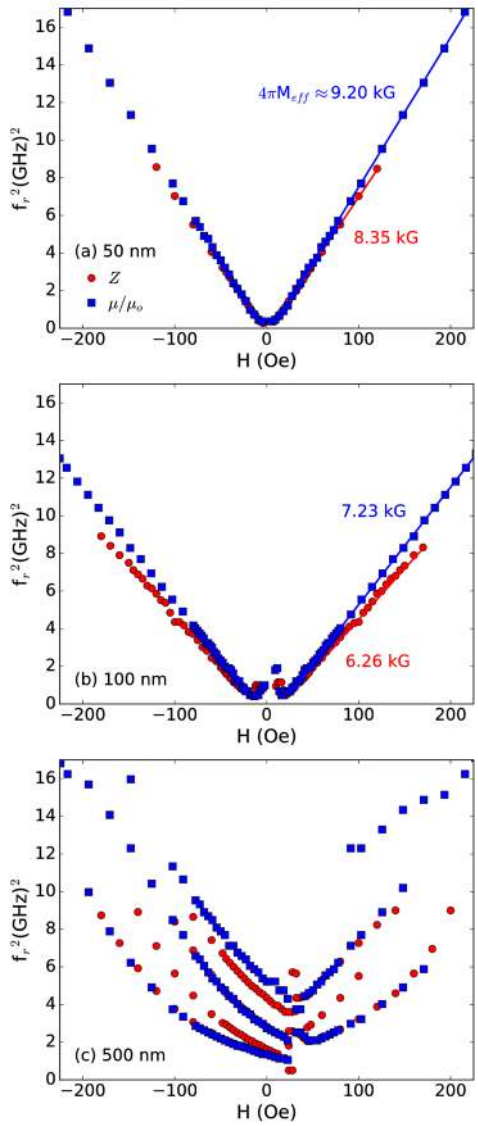

Figure 10. Dispersion relations obtained from the results of impedance Z and relative magnetic permeability μ/μ_o, $\phi = 0°$, for NiFe films with selected thicknesses. In particular, although the Z and μ/μ_o curves are acquired over a complete magnetization loop, here we show just part of the respective dispersion relations, obtained when the field goes from negative to positive values. The solid lines are linear fits of the dispersion relations at high field, obtained using equation (3), whose slope is associated to the effective magnetization $4\pi M_{\text{eff}}$ of the films.

dependent on the quasi-static magnetic field. Moreover, the remarkable asymmetric behavior in the dispersion relations also evidences the magnetization reversal process and the presence of magnetic domain structure, since the sample is not magnetically saturated. We point out that the curves are obtained from measurements with increasing fields, in which the field starts from a maximum negative value and is varied up to the maximum positive one. In particular, when the field goes from positive to negative values, the dispersion relations and the asymmetric behavior are reversed due to the magnetization reversal process in the descending branch of the magnetization loop.

The linear dependence of f_r^2 with H is expected just when the film is magnetically saturated. In particular, this fact is confirmed for films below 150 nm, which have a square magnetization loop, with low $H_s \approx H_c$. For the thicker films, linear dependence is just verified in a very restricted range at high magnetic field values, above H_s. Consequently, the limited range is not suitable for obtaining a precise and reliable estimation of $4\pi M_{\text{eff}}$. On the other hand, the dispersion relations clearly evidence that the multiple peaks structure, verified in the Z and μ/μ_o results, is directly related to the FMR effect. This is in concordance with previous studies reported in literature, in which experiments of zero-field dynamic permeability [6, 36], FMR [54, 71] and dynamic micromagnetic approach [52] exhibit spectra with several absorption peaks for films with thicknesses above the critical range.

4. Conclusion

In conclusion, we have investigated the thickness dependence of the magnetic anisotropy and dynamic magnetic response of ferromagnetic NiFe films with thicknesses in the range between 50 and 1000 nm. Firstly we have characterized the films from structural and morphological point of views, as well as investigating the quasi-static magnetic behavior. Our achievements show remarkable modifications in the magnetic anisotropy and magnetic properties with the film thickness. In a second moment, we have moved forward and investigated the dynamic magnetic response by means of three complementary techniques: the FMR, MI and magnetic permeability measurements.

From the results obtained through this experimental investigation, we have verified an increase of the crystalline grain size with thickness, although no evidence of evolution of the texture has been found. Moreover, we have split the films with different thicknesses into two groups according to the magnetic properties, and revealed the increase of the complexity of the whole sample as the film thickness is raised. For our set of films, there is a change of magnetic behavior for the critical thickness range between 150 and 200 nm. Films with thicknesses below 150 nm exhibit behavior of a classical in-plane uniaxial magnetic anisotropy system. In particular, they present two resonance modes in the FMR experiment, except the 50 nm-thick film, as well as a double peak structure in the MI effect and magnetic permeability curves. For films thicker than 200 nm, the quasi-static magnetization measurements indicate isotropic in-plane magnetic properties with an out-of-plane anisotropy contribution. This behavior is related to the emergence of a non-homogeneous magnetization configuration and local anisotropies arisen as a consequence of the non-uniformities of the stress stored in the film as the thickness is increased and/or to the columnar growth of the film. Such properties lead to spectra with two resonance modes in the FMR experiment that eventually overlap and merge as the thickness is increased. Similarly, the magnetoimpedance effect and magnetic permeability curves exhibit a complex magnetic behavior, depicted by several resonance peaks detected at relatively low fields, whose number raises with increasing the film thickness.

The approach considering FMR, MI and magnetic permeability measurements allowed us to obtain a broad magnetic characterization, revealing information on saturated and unsaturated states. The comparison of the results determined through the three techniques reveals good agreement between them. Although the techniques share the same magnetic fields configuration, they works at distinct frequency ranges and magnetic field amplitudes, as well as the experiments are performed with different setups and, consequently, may induce dissimilar distributions of alternating magnetic fields probing the sample. This may be the probable reason for the small discrepancies of the $4\pi M_{\text{eff}}$ values verified for the thinner films, and for the different number of resonance peaks verified in the dispersion relations obtained from the Z and μ/μ_o results, especially verified for the thicker films. Thus, we understand that these techniques provide complementary information on the magnetic anisotropy and dynamic magnetic response of the films.

These results correspond to a further step to understand the relations among thickness, magnetic anisotropy and dynamic magnetic response in films. Considering this fact, in order to obtain a complete general framework on the complex magnetic behavior in films with different thicknesses, more theoretical and experimental works are needed, not only performing studies using distinct techniques, but also considering techniques working together. We hope our results motivate both theoreticians and experimentalists.

Acknowledgments

We would like to thank I Z Damasceno for the experimental support and fruitful suggestions. The research is supported by the Brazilian agencies CNPq (Grants No. 306423/2014-6, No. 306362/2014-7, No. 441760/2014-7, No. 152650/2016-4), CAPES and FAPERN (Pronem No. 03/2012).

References

[1] Wolf S A 2001 *Science* **294** 1488–95
[2] Žutić I, Fabian J and Sarma S D 2004 *Rev. Mod. Phys.* **76** 323–410
[3] Phan M H and Peng H X 2008 *Prog. Mater. Sci.* **53** 323–420
[4] Ohring M 2007 *Handbook of Magnetism and Advanced Magnetic Materials* (New York: Wiley)
[5] Chopra K L and Kaur I 1983 *Thin Film Device Applications* (New York: Plenum)
[6] Viegas A D C, Correa M A, Santi L, da Silva R B, Bohn F, Carara M and Sommer R L 2007 *J. Appl. Phys.* **101** 033908
[7] da Silva R B, Corrêa M A, Silva E F, Mori T J A, Della Pace R D, Dutra R, Viegas A D C, Bohn F and Sommer R L 2014 *Appl. Phys. Lett.* **104** 102405
[8] Silva E F, Gamino M, de Andrade A M H, Corrêa M A, Vázquez M and Bohn F 2014 *Appl. Phys. Lett.* **105** 102409
[9] Fermin J R, Lucena M A, Azevedo A, de Aguiar F M and Rezende S M 2000 *J. Appl. Phys.* **87** 6421–3
[10] Rezende S, Lucena M, Azevedo A, Oliveira A, de Aguiar F and Egelhoff W 2001 *J. Magn. Magn. Mater.* **226–30** 1683–5
[11] Rodríguez-Suárez R L, Rezende S M and Azevedo A 2005 *Phys. Rev.* B **71** 224406
[12] Rodríguez-Suárez R L, Oliveira A B, Rezende S M and Azevedo A 2006 *J. Appl. Phys.* **99** 08R506
[13] Díaz de Sihues M, Durante-Rincón C and Fermin J 2007 *J. Magn. Magn. Mater.* **316** e462–5
[14] Rodríguez-Suárez R L, Vilela-Leão L H, Bueno T, Oliveira A B, de Almeida J R L, Landeros P, Rezende S M and Azevedo A 2011 *Phys. Rev.* B **83** 224418
[15] Vukadinovic N, Labrune M, Youssef J B, Marty A, Toussaint J C and Le Gall H 2001 *Phys. Rev.* B **65** 054403
[16] Belmeguenai M, Zighem F, Woltersdorf G, Roussigné Y, Chérif S M, Westerholt K and Bayreuther G 2009 *J. Magn. Magn. Mater.* **321** 750–3
[17] Raub C J 1993 *Handbook of Magnetic Materials* vol 6 (Amsterdam: Elsevier)
[18] Ciureanu P, Britel M, Menard D, Yelon A, Akyel C, Rouabhi M, Cochrane R W, Rudkowski P and Strom-Olsen J O 1998 *J. Appl. Phys.* **83** 6563–5
[19] Morrish A H 2001 *The Physical Principles of Magnetism* (New York: IEEE)
[20] Yin Y *et al* 2015 *Phys. Rev.* B **92** 024427
[21] Soonchul J, Choi Y and Ryu S 1997 *IEEE Trans. Magn.* **33** 3634–6
[22] Aitlamine H, Abelmann L and Puchalska I B 1992 *J. Appl. Phys.* **71** 353–61
[23] Rezende S M, Moura J A S, de Aguiar F M and Schreiner W H 1994 *Phys. Rev.* B **49** 15105–9
[24] Oliveira A B, Rodriguez-Suarez R L, Michea S, Vega H, Azevedo A, Rezende S M, Aliaga C and Denardin J 2014 *J. Appl. Phys.* **116** 033910
[25] Bekker V, Seemann K and Leiste H 2004 *J. Magn. Magn. Mater.* **270** 327–32
[26] Kern P, da Silva O, de Siqueira J, Pace R D, Rigue J and Carara M 2016 *J. Magn. Magn. Mater.* **419** 456–63
[27] Patterson A L 1939 *Phys. Rev.* **56** 978–82
[28] Cullity B D 1972 *Introduction to Magnetic Materials* (New York: Addison-Wesley)
[29] Sharma P and Gupta A 2006 *Nucl. Instrum. Methods Phys. Res.* B **244** 105–9
[30] Alves T M L, Bezerra C G, Viegas A D C, Nicolodi S, Corrêa M A and Bohn F 2015 *J. Appl. Phys.* **117** 083901
[31] Corrêa M A, Bohn F, Escobar V M, Marques M S, Viegas A D C, Schelp L F and Sommer R L 2011 *J. Appl. Phys.* **110** 093914
[32] de Andrade A M H, Corrêa M A, Viegas A D C, Bohn F and Sommer R L 2014 *J. Appl. Phys.* **115** 103908
[33] Corrêa M A, Bohn F, da Silva R B and Sommer R L 2014 *J. Appl. Phys.* **116** 243904
[34] Smith D O, Cohen M S and Weiss G P 1960 *J. Appl. Phys.* **31** 1755–62
[35] Nibarger J P, Lopusnik R, Celinski Z and Silva T J 2003 *Appl. Phys. Lett.* **83** 93–5
[36] Youssef J B, Vukadinovic N, Billet D and Labrune M 2004 *Phys. Rev.* B **69** 174402
[37] Hubert A and Schäfer R 1998 *Magnetic Domains: the Analysis of Magnetic Microstructures* (New York: Springer)
[38] Santi L, Bohn F, Viegas A D C, Durin G, Magni A, Bonin R, Zapperi S and Sommer R L 2006 *Physica* B **384** 144–6
[39] Coisson M, Celegato F, Olivetti E, Tiberto P, Vinai F and Baricco M 2008 *J. Appl. Phys.* **104** 033902
[40] Svalov A V, Aseguinolaza I R, Garcia-Arribas A, Orue I, Barandiaran J M, Alonso J, FernÁndez-Gubieda M L and Kurlyandskaya G V 2010 *IEEE Trans. Magn.* **46** 333–6
[41] Klemmer T J, Ellis K A, Chen L H, van Dover B and Jin S 2000 *J. Appl. Phys.* **87** 830
[42] Coïsson M, Appino C, Celegato F, Magni A, Tiberto P and Vinai F 2008 *Phys. Rev.* B **77** 214404
[43] Spain R J 1963 *Appl. Phys. Lett.* **3** 208–9
[44] Fujiwara H, Sugita Y and Saito N 1964 *Appl. Phys. Lett.* **4** 199

[45] Leva E S, Valente R C, Tabares F M, Mansilla M V, Roshdestwensky S and Butera A 2010 *Phys. Rev.* B **82** 144410
[46] Soh W T, Phuoc N N, Tan C Y and Ong C K 2013 *J. Appl. Phys.* **114** 053908
[47] Amos N, Fernandez R, Ikkawi R, Lee B, Lavrenov A, Krichevsky A, Litvinov D and Khizroev S 2008 *J. Appl. Phys.* **103** 07E732
[48] Corrêa M A, Bohn F, Chesman C, da Silva R B, Viegas A D C and Sommer R L 2010 *J. Phys. D: Appl. Phys.* **43** 295004
[49] Papanikolaou S, Bohn F, Sommer R L, Durin G, Zapperi S and Sethna J P 2011 *Nat. Phys.* **7** 316–20
[50] Bohn F, Corrêa M A, Viegas A D C, Papanikolaou S, Durin G and Sommer R L 2013 *Phys. Rev.* E **88** 032811
[51] Bohn F, Corrêa M A, Carara M, Papanikolaou S, Durin G and Sommer R L 2014 *Phys. Rev.* E **90** 032821
[52] Vukadinovic N, Vacus O, Acher O and Pain D 2000 *Phys. Rev. Lett.* **85** 2817–20
[53] Cheng S F, Lubitz P, Zheng Y and Edelstein A S 2004 *J. Magn. Magn. Mater.* **282** 109–14
[54] Ramos C A, Brigneti E V, Gómez J and Butera A 2009 *Physica* B **404** 2784–6
[55] Fermin J R *et al* 1999 *J. Appl. Phys.* **85** 7316–20
[56] Samantaray B, Singh A K, Banerjee C, Barman A, Perumal A and Mandal P 2016 *IEEE Trans. Magn.* **52** 1–4
[57] Martins A, Trippe S, Santos A and Pelegrini F 2007 *J. Magn. Magn. Mater.* **308** 120–5
[58] Sparks M 1970 *Phys. Rev.* B **1** 3869–80
[59] Smit J and Beljers H G 1955 *Phillips Res. Rep.* **10** 113–30
[60] Belmeguenai M, Zighem F, Roussigné Y, Chérif S M, Moch P, Westerholt K, Woltersdorf G and Bayreuther G 2009 *Phys. Rev.* B **79** 024419
[61] Gallardo R A, Banholzer A, Wagner K, Körner M, Lenz K, Farle M, Lindner J, Fassbender J and Landeros P 2014 *New J. Phys.* **16** 023015
[62] Chen Y C, Hung D S, Yao Y D, Lee S F, Ji H P and Yu C 2007 *J. Appl. Phys.* **101** 09C104
[63] Gubbiotti G, Tacchi S, Carlotti G, Vavassori P, Singh N, Goolaup S, Adeyeye A O, Stashkevich A and Kostylev M 2005 *Phys. Rev.* B **72** 224413
[64] Dumas R K, Iacocca E, Bonetti S, Sani S R, Mohseni S M, Eklund A, Persson J, Heinonen O and Åkerman J 2013 *Phys. Rev. Lett.* **110** 257202
[65] Kraus L 2003 *Sensors Actuators* A **106** 187–94
[66] Kraus L 1999 *J. Magn. Magn. Mater.* **195** 764–78
[67] Sommer R L and Chien C L 1995 *Appl. Phys. Lett.* **67** 3346
[68] Barandiarán J M, García-Arribas A and De Cos D 2006 *J. Appl. Phys.* **99** 103904
[69] Banerjee C, Chaurasiya A K, Saha S, Sinha J and Barman A 2015 *J. Phys. D: Appl. Phys.* **48** 395001
[70] Kittel C 2004 *Introduction to Solid State Physics* (New York: Wiley)
[71] Ebels U, Buda L, Ounadjela K and Wigen P 2001 *Phys. Rev.* B **63** 1–11